Appl. Phys. B 81, 13–17 (2005)
DOI: 10.1007/s00340-005-1878-2

Applied Physics B
Lasers and Optics

X. ZHOU[1,✉]
T. KANAI[1]
D. YOSHITOMI[1,2]
T. SEKIKAWA[1]
S. WATANABE[1]

Generation of high average power, 7.5-fs blue pulses at 5 kHz by adaptive phase control

[1]Institute for Solid State Physics, University of Tokyo, 5-1-5 Kashiwanona, Kashiwa 277-8581, Japan
[2]National Institute of Advanced Industrial Science and Technology, 1-1-4 Umezono, Tsukuba 305-8568, Japan

Received: 25 November 2004 /
Revised version: 25 April 2005
Published online: 14 June 2005 •

ABSTRACT The spectral width of a 5-kHz Ti:sapphire laser system was broadened by spectral control in a regenerative amplifier consisting of broadband chirped mirrors. The dispersion over the wide spectral range was compensated by a deformable mirror along with a genetic algorithm, resulting in a pulse width of 15 fs. The pulse width is the shortest, to our knowledge, in chirped pulse amplification systems with a regenerative amplifier. The phase distortion of broadband frequency doubling in addition to the Ti:sapphire laser was compensated by using the self-diffraction intensity in sapphire as the feedback signal into the genetic algorithm, resulting in a pulse width of 7.5 fs. The average power of the second harmonic was 1 W with a fundamental input of 7 W.

PACS 42.55.-f; 42.65.Ky; 42.65.Re

1 Introduction

Intense ultra-short pulses at a high repetition rate have opened the way to attosecond pulses in the XUV and soft X-ray region. Isolated attosecond pulses were demonstrated in the harmonic continuum around 13 nm by using carrier-envelope-phase-stabilized, few-cycle pulses [1]. We have recently generated isolated attosecond pulses from a single harmonic by another method where the harmonic was generated in the nonadiabatic regime by the rising part of driving pulses and shut off by full ionization [2]. In this scheme, an ultra-short-pulse, short-wavelength laser played an essential role because the pulse rise should be steep and the spectral separation between the neighboring harmonics should be wide enough to prevent the spectral overlap.

We reported the generation of subterawatt sub-10-fs blue pulses by broadband frequency doubling (BFD) [3] and compensated the pulse-front distortion due to a single-lens BFD system [4]. However, the shortest pulse obtained was limited to 8.3 fs mainly because of the fundamental pulse width [2, 3]. Obviously, the spectral broadening along with adaptive phase compensation is necessary for further pulse shortening.

✉ Fax: +81-4-7136-3362, E-mail: zxy@issp.u-tokyo.ac.jp

In this paper, the spectral width of a 5-kHz Ti:sapphire laser system was broadened by spectral control with two etalons and spatial masks in the regenerative amplifier consisting of broadband chirped mirrors. The dispersion over the wide spectral range was compensated by a deformable mirror (DM) along with a genetic algorithm (GA), resulting in a pulse width of 15 fs. The pulse width is the shortest in the chirped pulse amplification (CPA) systems with a regenerative amplifier [5], although similar [6] or shorter pulses [7] were obtained by multipass amplifiers alone. Next, the BFD system in addition to the Ti:sapphire laser was phase compensated by using the self-diffraction intensity as the feedback signal into the genetic algorithm. The pulse width was 7.5 fs. The average power of the second harmonic was 1 W with a fundamental input of 7 W. This average power is higher by almost two orders of magnitude than those obtained by using hollow fibers in the short-wavelength region [8, 9].

In this paper, we describe a 5-kHz CPA laser system in Sect. 2.1, spectral broadening and phase compensation in the fundamental beam in Sect. 2.2 and phase compensation in BFD in Sect. 3.

2 Adaptive phase control in the fundamental beam

2.1 *5-kHz CPA laser system*

A 5-kHz CPA Ti:sapphire system with an adaptive phase controller was used in this experiment. The 5-kHz amplifier system is shown schematically in Fig. 1 [10, 11], which consists of a mode-locked oscillator, an Offner-type stretcher, a regenerative amplifier, a four-pass amplifier, a single-pass amplifier and a compressor. The oscillator generates 12-fs (FWHM) pulses at 75 MHz. The pulses were stretched to ∼ 400 ps by an Offner-type stretcher with a single 1200-grooves/mm grating and sent to the regenerative amplifier. The regenerative amplifier consists of an x-folded cavity with two flat mirrors and two concave mirrors. The cavity of the regenerative amplifier contains a Pockels cell driven by a triode unit with a pre-bias module, a 12-mm-long Ti:sapphire crystal, a thin-film polarizer and a LAH64 glass-prism pair. The prism pair was used to compensate the high-order dispersions. The Ti:sapphire crystal was pumped by the second harmonic (SH) of a Q-switched Nd:YAG laser at 5 kHz. The single pulse was extracted after 15 round trips from the regenerative amplifier and sent to the multipass amplifier.

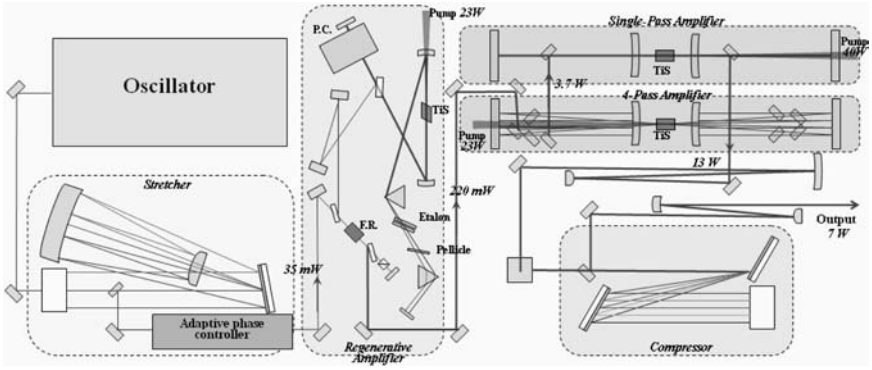

FIGURE 1 Schematic diagram of a 5-kHz amplifier system. P.C.: Pockels cell, F.R.: Faraday rotator, TiS: Ti:sapphire. The system consists of a mode-locked oscillator, an Offner-type stretcher, a regenerative amplifier, a four-pass amplifier, a single-pass amplifier and a compressor

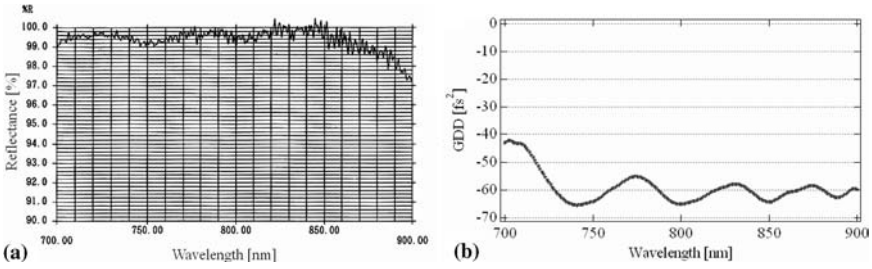

FIGURE 2 The reflectance and the group-delay dispersion of a broadband chirped mirror. **a** The measured reflectance. The reflectance is above 99% from 700 nm to 880 nm. **b** The calculated group-delay dispersion of the chirped mirror

The 30-mm-long Ti:sapphire crystals in the two amplifiers at a later stage were pumped by the SH of a Q-switched Nd:YAG laser. After four-pass and single-pass amplification, the pulse was finally sent to the compressor. The second- and third-order dispersions were balanced over the given spectrum by the compressor along with the prism pair in the regenerative amplifier. The pulse width was 22 fs [10, 11].

2.2 *Spectral broadening and adaptive phase control in the fundamental beam*

The broader spectral width and the compensation of higher-order dispersion are necessary to realize the further pulse shortening. The spectrum of the pulse is from 720 nm to 870 nm after the stretcher, although the edge of the spectrum is lost because of the limited width of the folding mirrors. However, the spectral narrowing occurs mainly in the regenerative amplifier because of gain narrowing and the limited bandwidth of the total reflectors (from 750 nm to 857 nm above 99% reflectance). We developed broadband chirped mirrors with the spectral range from 700 nm to 880 nm above 99% reflectance (Fig. 2a). Then, the four mirrors in the regenerative amplifier were replaced by the broadband chirped mirrors. The group-delay dispersion (GDD) of the chirped mirror is about $-60\,\mathrm{fs}^2$ over the above spectral range (Fig. 2b). The negative GDD is not important because the total GDD is much larger ($1.77 \times 10^6\,\mathrm{fs}^2$). The reason why we adopted the chirped mirror is that it gave a high reflectance and a flat GDD over a spectral range wider than a dispersion-less mirror.

A 2-μm-thick pellicle beam splitter was added to the air-spaced etalon whose space is controlled by a piezo-electric actuator to improve the spectral broadening [5, 12]. The pellicle and etalons were inserted between the prisms because there was no other space to accommodate them. In addition, spatial masking was performed for spectral shaping between the prism pair and the total reflector, where the spectrum is spatially separated with a parallel beam, in the regenerative amplifier. Three needles were inserted in the positions corresponding to the arrows in Fig. 3. The spectrum of the regenerative amplifier is shown in Fig. 3 along with the transform-limited pulse shape. The amplified spectrum covers from 737 nm to 865 nm, resulting in a spectral width of 115 nm (FWHM). The Fourier transform of the spectrum gives a pulse width (FWHM) of 14 fs.

The phase distortion over such a wide spectrum cannot be compensated by the grating pair in the compressor and the prism pair in the generative amplifier. The dispersion including higher orders over the wide spectrum was compensated by using a deformable mirror in this experiment [6, 13].

The deformable mirror consists of a gold-coated silicon nitride membrane (OKO Technologies). The surface is driven electrostatically by 2×19 rows of electrodes. The aperture of the deformable mirror is $11 \times 39\,\mathrm{mm}^2$. Because the gold-coated DM cannot be used for the amplified pulse, we

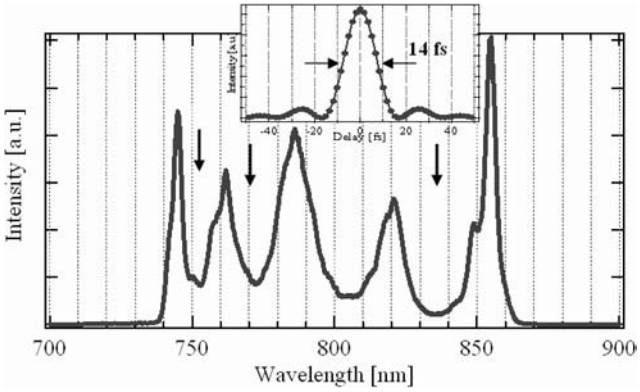

FIGURE 3 Spectrum of the amplified pulse. The FWHM of the amplified spectrum is about 115 nm. The *arrows* correspond to the positions of needles. The Fourier transform of the spectrum gives a pulse width (FWHM) of 14 fs (*inset*)

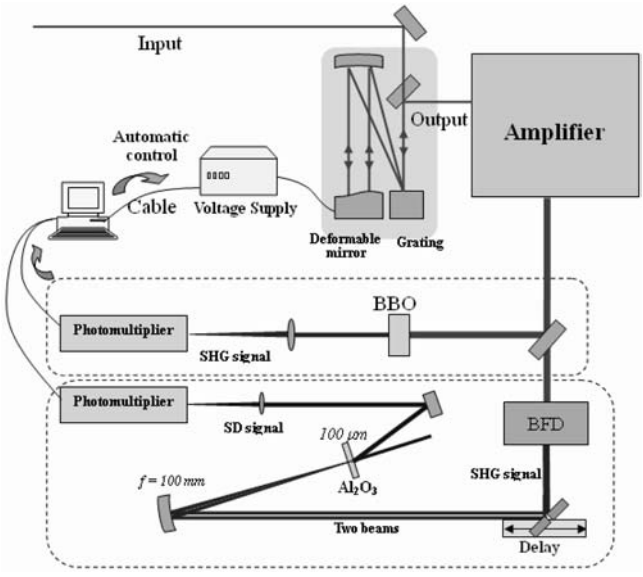

FIGURE 4 Experimental setup for adaptive phase control. The deformable mirror was used as a phase modulator to compensate the higher-order dispersion along with an iterative genetic algorithm. For the feedback to the genetic algorithm, the algorithm sampled the parameter space to maximize the second-harmonic (SH) and self-diffraction (SD) intensities for the fundamental and second-harmonic pulses, respectively

placed the DM system between the stretcher and the regenerative amplifier. Here, the Faraday rotator and polarizer were used to avoid feedback from the amplifier to the oscillator.

The phase compensator with the deformable mirror and a grating is shown in Fig. 4 along with the control procedure. The output from the stretcher was angularly dispersed by a 300-grooves/mm grating. The frequency components were spatially separated horizontally and Fourier transformed by a concave mirror ($R = 0.6$ m) on the deformable mirror. After the reflection by the deformable mirror, the beam returned to the concave mirror and grating and was collimated to the initial spot. The phase of the reflected beam was modulated by the deformable mirror.

The voltages of the actuator electrodes can be controlled from 0 to 285 V. Both ends of the mirror are fixed on the base. When all of the actuators are set to 0 V, the surface of the deformable mirror is almost flat. The advantage of the deformable mirror over a liquid-crystal modulator is smooth phase modulation. However, an individual actuator cannot be controlled independently from the neighboring actuators, and cannot be adjusted by the applied voltage to the calculated shape. Then, we adopted a genetic algorithm (GA) [6, 13–15] to search for the best surface shape of the deformable mirror. Because the surface of the deformable mirror can only be pulled by the actuators, the mirror cannot be set to be a convex mirror. Thus, the initial position of the mirror surface was set to be a concave mirror with all the actuators set to 100 V.

For the feedback to the genetic algorithm, the amplified pulse was focused by a lens into a 50-μm-thick BBO crystal, generating a second-harmonic signal. The signal detected by a photomultiplier was digitized and sent to a computer. The algorithm sampled the parameter space to maximize the SH output. The best solution (10 parents) generated the next set of possible solutions (100 children) in each iteration. The actuator voltages and the fitness value were the only parameters needed by the GA.

The convergence of the GA is not so good because of the fluctuation in the laser intensity. Then, we adopted two steps to operate the GA program. We increased the mutation quantity (variable from 0 to 255) and the mutation probability (variable from 0 to 100%) in the mutation step for coarse search. This also avoids the fall in the local maxima. Second, we reduced the mutation quantity and the mutation probability for fine search, and operated the program with the solution of the first step as the initial population.

After running the optimization algorithm for about 40 min, the SH signal increased and began to stagnate. Figures 5 and 6 show second-harmonic-generation (SHG) frequency-resolved optical gating (FROG) measurements [16] of the output pulse shapes without and with adaptive control, respectively. In both figures (a) and (b) show the SHG-FROG trace and the retrieved pulse shape with the associated phase, respectively. After adaptive phase control, the phase became flatter and the side bumps were reduced, resulting in the reduction of the pulse width from 19 fs to 15 fs. The measured pulse width of 15 fs is a little longer than the transform limit (14 fs). This may be due to the incomplete phase compensation or due to the broadband component of amplified spontaneous emission from the regenerative amplifier.

3 Adaptive phase control in the SH beam

3.1 *Broadband frequency doubling*

If the whole spectral components of a square spectrum are frequency doubled, the frequency width of the second harmonic (SH) becomes twice that of the fundamental,

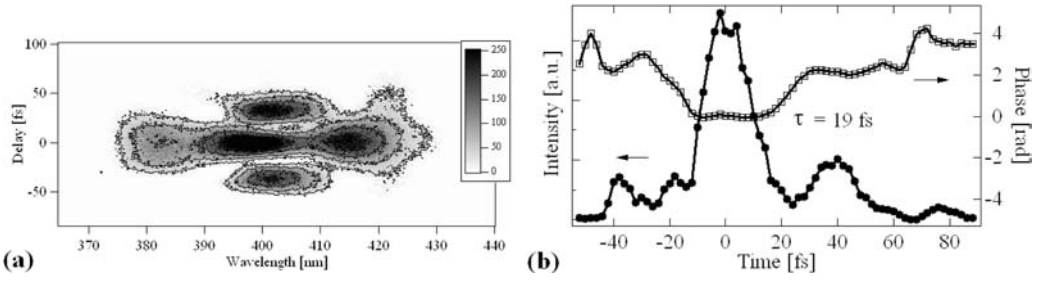

FIGURE 5 Second-harmonic frequency-resolved optical gating measurement of the fundamental output pulse without adaptive control. **a** FROG trace. **b** Retrieved pulse shape and phase

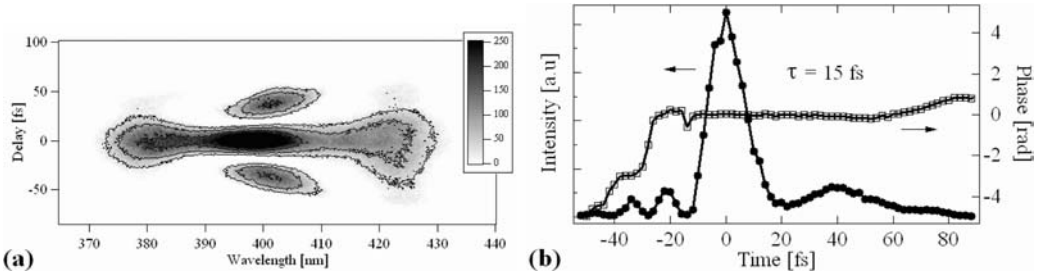

FIGURE 6 Second-harmonic frequency-resolved optical gating measurement of the fundamental output pulse with adaptive control. **a** FROG trace. **b** Retrieved pulse shape and phase

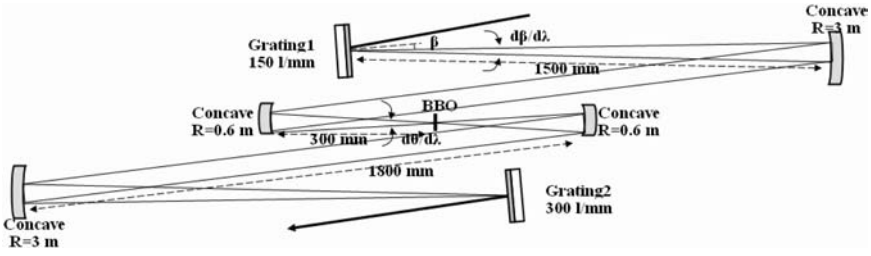

FIGURE 7 Schematic of modified broadband frequency-doubling system. β: diffraction angle; $d\beta/d\lambda$: the angular dispersion of the grating; $d\theta/d\lambda$: the wavelength dispersion of the phase-matching angle

making the SH pulse width half of the fundamental. This is also valid for the spectrum of Fig. 3 having sharp edges at both spectral ends. The broadband frequency doubling (BFD) scheme was proposed and demonstrated [3, 17, 18]. The experimental setup of BFD is shown in Fig. 7. The dispersion of the phase-matching angle ($d\theta/d\lambda$) is given by the angular dispersion ($d\beta/d\lambda$) of the grating (G1) with a magnification factor (M), i.e. $d\theta/d\lambda = (d\beta/d\lambda)/M$, where $M = 0.2$. The telescope with two concave mirrors was used for image relay instead of a single lens to eliminate the pulse-front distortion due to aberration [4]. The optical configuration after the BBO crystal is symmetrical to that before the BBO crystal except for the twice greater groove density of G2, which compensates the angular dispersion. The thickness of the BBO crystal was 300 μm or 150 μm.

3.2 *Adaptive phase control in the SH*

The full spectral width of a 15-fs pulse in Fig. 6 is about 100 nm (from 750 nm to 850 nm), while the full acceptable spectral widths of BFD are 127 nm and 179 nm, respectively, for 300-μm and 150-μm-thick BBO crystals. Then, the second-order dispersion of the phase-matching angle was not taken into account. In BFD, the extra dispersion from the BBO crystal, mirrors and gratings is added to the fundamental Ti:sapphire system. Then, adaptive compensation should be done in the total system. As shown in Fig. 4, the total self-diffraction intensity in a 100-μm-thick sapphire plate was used as the feedback signal to the GA. The procedure of phase compensation with a GA is the same as in the fundamental beam as described above. The SD spectrum can be fed to the GA and may give us a more robust search algorithm. However, this was not attempted in this paper. The relative delay between the two beams was always fixed so as to give the maximum signal and is not changed by the form of the DM because it does not change the spatial shape of the beam. The coarse adjustment was done by changing the grating separation in the compressor of the Ti:sapphire system.

Frequency-resolved optical gating was performed by using the self-diffraction signal from a sapphire plate [8, 9, 19]. Figure 8 shows (a) the measured and (b) the retrieved FROG traces. The RMS error was 2%. Figure 9 shows the retrieved pulse shape with the corresponding phase. The angle of the two beams was 2.9° and the confocal parameter was 50 μm with the beam diameter of 1 cm. The wavelength dependence

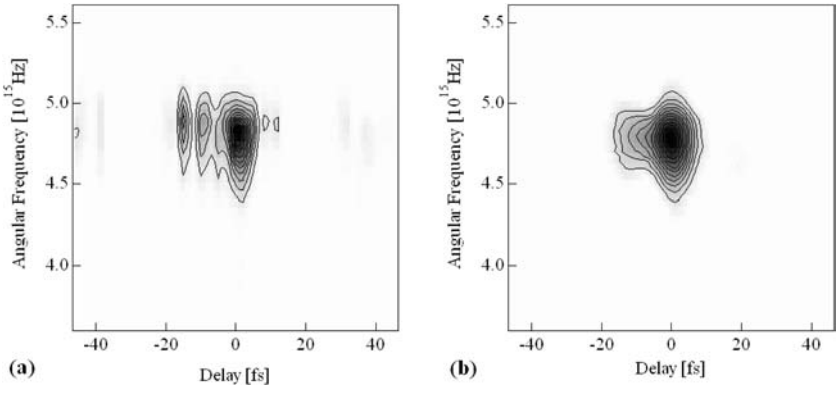

FIGURE 8 The measured (**a**) and retrieved (**b**) SD-FROG traces of the second-harmonic pulse

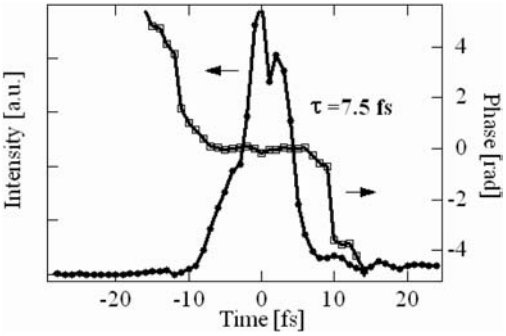

FIGURE 9 The retrieved pulse shape and phase of the second-harmonic pulse by self-diffraction frequency-resolved optical gating

of the conversion efficiency from the input to the SD signal was calculated by combining the ω^2 dependence with phase matching in this condition [20]. This spectral filtering effect shows a gradual increase by about 20% from 430 nm to 370 nm for the interaction lengths of 100 μm (the crystal thickness) and 50 μm (the confocal parameter). The correction of this effect does not change the retrieved pulse shape. However, this effect becomes more serious with decreasing pulse width. The pulse width of 7.5 fs is half of the fundamental pulse width (15 fs) from Fig. 9. The retrieved spectrum reflects quite well the typical measured spectrum.

The output power from BFD was 1 W by using a 300-μm-thick BBO crystal when the input power was 7 W with a beam diameter of 12 mm. The output powers and the pump powers at the intermediate stage are already shown in Fig. 1.

4 Conclusion

We have developed a broadband Ti:sapphire amplifier system with an adaptive phase controller. Broadband chirped mirrors were used in the regenerative amplifier. The output spectrum from the regenerative amplifier was shaped with a thin-film polarizer etalon and a pellicle beam splitter in addition to a spatial mask. A deformable mirror was used as a phase modulator to compensate the higher-order dispersion along with an iterative genetic algorithm. The pulse width was 15 fs. The second harmonic was generated by broadband frequency doubling. The phase distortion of the total system was compensated by using a self-diffraction intensity as a feedback signal to the genetic algorithm. Frequency-resolved optical gating measurements revealed that the pulse duration of the SH was 7.5 fs. This scheme will be extended to 1-kHz [21] and 10-Hz systems [22] to obtain subterawatt and terawatt peak powers.

REFERENCES

1 R. Kienberger, E. Goulielmakis, M. Uiberacker, A. Baltuska, V. Yakovlev, F. Bammer, A. Scrinzi, T. Westerwalbesloh, U. Kleineberg, U. Heinzmann, M. Drescher, F. Krausz, Nature **427**, 817 (2004)
2 T. Sekikawa, A. Kosuge, T. Kanai, S. Watanabe, Nature **432**, 605 (2004)
3 T. Kanai, X. Zhou, T. Sekikawa, S. Watanabe, T. Togashi, Opt. Lett. **28**, 1484 (2003)
4 T. Kanai, X. Zhou, T. Liu, A. Kosuge, T. Sekikawa, S. Watanabe, Opt. Lett. **29**, 2929 (2004)
5 Y. Nabekawa, Y. Shimizu, K. Midorikawa, Opt. Lett. **27**, 1265 (2002)
6 E. Zeek, R. Bartels, M. Murnane, H.C. Kapteyn, S. Backus, Opt. Lett. **25**, 587 (2000)
7 H. Takada, M. Kakehata, K. Torizuka, in *Ultrafast Optics IV*, ed. by F. Krausz, G. Korn, P. Corkum, I.A. Walmsley (Springer, Berlin, 2004), p. 85
8 O. Duhr, E.T.J. Nibbering, G. Korn, Opt. Lett. **24**, 34 (1999)
9 C.G. Durfee III, S. Backus, H.C. Kapteyn, M.M. Murnane, Opt. Lett. **24**, 697 (1999)
10 Y. Nabekawa, T. Togashi, T. Sekikawa, S. Watanabe, S. Konno, T. Kojima, S. Fujikawa, K. Yasui, Appl. Phys. B **70**, S171 (2000)
11 Y. Nabekawa, T. Togashi, T. Sekikawa, S. Watanabe, S. Konno, T. Kojima, S. Fujikawa, K. Yasui, Opt. Express **5**, 318 (1999)
12 K. Yamakawa, C.P.J. Barty, Opt. Lett. **28**, 2402 (2003)
13 E. Zeek, K. Maginnis, S. Backus, U. Russek, M.M. Murnane, G. Mourou, H. Kapteyn, Opt. Lett. **24**, 493 (1999)
14 O. Albert, H. Wang, D. Liu, Z. Chang, G. Mourou, Opt. Lett. **25**, 1125 (2000)
15 D. Meshulach, D. Yelin, Y. Silberberg, J. Opt. Soc. Am. B **15**, 1615 (1998)
16 D.J. Kane, R. Trebino, IEEE J. Quantum Electron. **29**, 571 (1993)
17 G. Szebo, Z. Bor, Appl. Phys. B **50**, 51 (1990)
18 O.E. Martinez, IEEE J. Quantum Electron. **25**, 2464 (1989)
19 T.S. Clement, A.J. Taylor, Opt. Lett. **20**, 70 (1995)
20 A. Baltuska, M.S. Pshenichnikov, D.A. Wiersma, in *Frequency-Resolved Optical Gating: The Measurement of Ultrashort Laser Pulses*, ed. by R. Trebino (Kluwer, Boston Dordrecht London, 2002), p. 286
21 Y. Nabekawa, Y. Kuramoto, T. Togashi, T. Sekikawa, S. Watanabe, Opt. Lett. **23**, 1384 (1998)
22 J. Itatani, Y. Nabekawa, K. Kondo, S. Watanabe, Opt. Commun. **134**, 134 (1997)